Magnetic Grüneisen parameter for model systems

Gabriel O. Gomes,[1,*] Lucas Squillante,[1] A. C. Seridonio,[2] Andreas Ney,[3] Roberto E. Lagos,[1] and Mariano de Souza [1,†]

[1]*Departamento de Física, São Paulo State University (UNESP), IGCE, Rio Claro, 13506-900 São Paulo, Brazil*
[2]*Faculdade de Engenharia de Ilha Solteira, São Paulo State University (UNESP), Ilha Solteira, 15385-000 São Paulo, Brazil*
[3]*Institute of Semiconductor and Solid State Physics, Johannes Kepler University Linz, 4040 Linz, Austria*

The magnetocaloric effect (MCE), which is the refrigeration based on the variation of the magnetic entropy, is of great interest in both technological applications and fundamental research. The MCE is quantified by the magnetic Grüneisen parameter Γ_{mag}. We report on an analysis of Γ_{mag} for the classical Brillouin-like paramagnet for a modified Brillouin function taking into account a zero-field splitting originated from the spin-orbit (SO) interaction and for the one-dimensional Ising (1DI) model under a longitudinal field. For the Brillouin-like model with SO interaction and the longitudinal 1DI model, a sign-change in the MCE is observed for vanishing T and B. SO interaction leads to a narrowing of the enhancement of Γ_{mag} for T and $B \rightarrow 0$. Our findings emphasize the relevance of Γ_{mag} for exploring critical points. Also, we show that the Brillouin model with and without SO interaction can be recovered from the 1DI model in the regime of high temperatures and vanishing coupling constant J.

I. INTRODUCTION

Although *classical* phase transitions are driven by thermal fluctuations [1], a genuine *quantum* phase transition (QPT) [2] takes place at $T = 0$ K. In this case, thermal fluctuations are absent, and the transition is driven by tuning a control parameter g (see Fig. 1), namely, application of external pressure, magnetic field, or changes in the chemical composition of the system of interest. Intricate manifestations of matter have been observed in the immediate vicinity of a quantum critical point (QCP) (cf. Fig. 1), i.e., the point in which the QPT takes place, such as divergence of the Grüneisen parameter computed by combining ultra-high-resolution thermal expansion and specific-heat measurements [3–5], collapse of the Fermi surface as detected via Hall-effect measurements [6], non-Fermi-liquid behavior observed by carefully analyzing the power law obeyed by the electrical resistivity, specific heat, magnetic susceptibility [7,8], and breakdown of the Wiedemann-Franz law due to an anisotropic collapse of the Fermi surface [9]. Hence, the exploration and understanding of the physical properties of interacting quantum entities on the verge of a QCP consist of topics of wide current interest, see, e.g., Ref. [10] and references therein. In this context, heavy-fermion compounds have been used as an appropriate platform to explore such exotic manifestations of matter [11]. Interestingly enough, new sorts of quantum critical behavior, having strong spin-orbit (hereafter SO) coupling and electron correlations as key ingredients, embodying an antiferromagnetic semimetal Weyl phase [15] and excitations of strongly entangled spins called spin orbitons [16], have been recently

reported in the literature. Furthermore, a QPT in graphene tuned by changing the slope of the Dirac cone has also been reported [17]. In general terms, the fingerprints of a magnetic-field-induced QPT are the divergence of the magnetic susceptibility [18] $\chi(T, B) = \mu_0(\partial M/\partial B)$ (here, M refers to the magnetization, B is an external magnetic field, and μ_0 is the vacuum permeability) for $T \rightarrow 0$ K and a sign change in the MCE near QCPs [19]. Indeed, such fingerprints have been observed experimentally in several materials. Among them are $YbRh_2Si_2$ [20], Cs_2CuBr_4 [21], and $CeCoIn_5$ [22], just to mention a few examples. Furthermore, zero-field QCPs have been also recently reported in the f-based superconductors $CeCoIn_5$ [23], β-$YbAlB_4$ [18], and quasicrystals of the series Au-Al-Yb [24]. Owing to the experimental difficulties posed by accessing a QCP under pressure and/or under an external magnetic field, zero-field QCPs are of high interest since quantum criticality is, thus, accessible simply by means of temperature sweeps. An analogous situation is encountered, for instance, in molecular conductors regarding the finite-T critical end point of the Mott metal-to-insulator transition [25–27] as well as for gases [28]. From the theoretical point of view, however, topics still under intensive debate are as follows: (i) the universality class of QPTs [11,27]; (ii) the temperature range of robustness of quantum fluctuations and the role played by them, for instance, in the mechanism behind high-temperature superconductivity [10]. Several theoretical models have been served as appropriated platforms to address these issues, being the transverse 1DI model, namely, an Ising chain under a transverse magnetic field, an appropriate playground to investigate several fundamental aspects [29,30]. Indeed, for the transverse 1DI model, exactly solved analytically, there is no spontaneous magnetization, and a phase transition occurs only at $T = 0$ K under a finite magnetic field [31], see Fig. 1. This is merely a direct consequence of the famous Mermin-Wagner theorem

---

*Present address: Department of Astronomy, University of São Paulo, São Paulo 05508-090, Brazil.
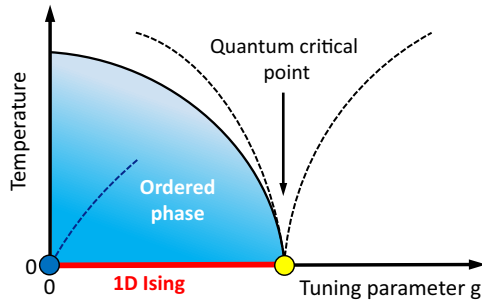†mariano.souza@unesp.br

FIG. 1. Schematic phase diagram of the temperature *versus* tuning parameter *g*, indicating two quantum critical points. Yellow and blue bullets indicate a magnetic-field-tuned and a zero-field QCP, respectively. The red line at $T = 0$ K depicts a magnetic-field-induced QPT for the transverse 1D Ising model. The dashed line for the hypothetical magnetic field-induced quantum critical point (yellow bullet) indicates the suppression of an energy scale, while the dashed line from the origin (blue bullet) represents the enhancement of the magnetic susceptibility for vanishing magnetic field [12]. In the case of a magnetic-field-induced QPT, the solid line refers to the adiabatic magnetization [13]. Figure adapted from Refs. [3,14]. Details in the main text.

[32], which forbids long-range magnetic ordering at finite temperatures in dimensions $d \leqslant 2$. Since the 1DI Hamiltonian considers solely nearest-neighbor interactions, computing the eigenenergy of a spin configuration is a relatively easy task [1]. As a matter of fact, in a broader context, thought the Ising model, at first glance, is a *toy model* to simulate a domain in a ferromagnetic material, it still continues to attract broad interest, for instance, in the field of quantum information theory [33] and detection of Majorana edge states [34]. Motivated by the intrinsic quantum critical nature of the 1DI model under a transverse field, we explore a possible similar behavior in other exactly analytically solvable models.

The focus of the present paper lies on the report of an intrinsic diverging magnetic Grüneisen parameter for the various model systems discussed here in the limit of a vanishing magnetic field and $T \rightarrow 0$. Following the discussions in Ref. [35] in order to probe a magnetic-field-induced QCP, the criteria to be fulfilled are based on particular behavior of the magnetic Grüneisen parameter Γ_{mag} as follows: (i) a divergence of Γ_{mag} for $T \rightarrow 0$; (ii) a sign change in Γ_{mag} upon crossing the critical magnetic-field B_c, and (iii) a typical $T/(B - B_c)^\epsilon$ scaling, where ϵ is the so-called scaling exponent. Our analysis on the magnetic Grüneisen parameter, to be discussed in the following, fulfill these criteria, being the investigation of the (iii) criterium out of the scope of the present paper [12]. For *real* materials, a divergence of the magnetic Grüneisen parameter for vanishing B and $T \rightarrow 0$ might be related to the presence of residual amount of magnetic moments [35]. Hence, the divergence of the Grüneisen ratio, namely, the ratio of the thermal expansion to specific heat, is also required to probe genuine quantum criticality [35]. In the case of an *ideal* paramagnet, upon approaching zero temperature and removing the external magnetic field, one achieves the limit where mutual interactions are relevant with a typical local magnetic field of about 0.01 T for a distance between neighboring electron's spins ($S = 1/2$) of 5 Å

as discussed in Ref. [36]. It turns out that one has an intrinsic entropy change for a vanishing external magnetic field [36]. Such entropy change is related to the enhancement of Γ_{mag} for B and $T \rightarrow 0$. Surprisingly enough, the model systems to be discussed in the following incorporate such features.

This paper is organized as follows: In Sec. II, the MCE is calculated for the classical Brillouin-like paramagnet; in Sec. III, the SO interaction is taken into account to calculate the MCE for the Brillouin paramagnet for $S = 3/2$, being the results compared with those obtained in Sec. II, the 1DI model under longitudinal field is recalled, and the corresponding MCE is presented in Sec. IV.

Before starting the discussions on the MCE for the Brillouin-like paramagnet, it is worth recalling that both 1DI and the two-dimensional Ising (2DI) models provide an appropriate playground to explore critical points both theoretical and experimentally. For zero external field $B = 0$ T, the model can be exactly solved, and it is known as the famous Onsager solution [1,37,38]. The mathematical solution of both 1DI and 2DI models in the absence of an external magnetic field can be found in classical textbooks, see, e.g., Refs. [31,39,40]. A hypothetical sample with a volume of 1 mm^3, the *Système International* values of $\mu_B = (9.27 \times 10^{-24})$ J T^{-1}, the Boltzmann constant $k_B = (1.38 \times 10^{-23})$ m^2 kg s^{-2} K^{-1}, and $N = (6.022 \times 10^{23})$ atoms were employed in the calculations. For the 1DI model, we have employed a magnetic coupling constant $J = 10^{-23}$ J $= 0.72$ K. Also, it is worth mentioning that the MCE is quantified by Γ_{mag}.

II. THE BRILLOUIN-LIKE PARAMAGNET

In what follows, we discuss the MCE for the Brillouin paramagnet. First, we recall the Brillouin function B_J, well known from textbooks [31]:

$$B_J(J, y) = \frac{2J+1}{2J}\coth\left(\frac{2J+1}{2J}y\right) - \frac{1}{2J}\coth\left(\frac{y}{2J}\right), \quad (1)$$

where $y = g_J \mu_B J B / k_B T$, g_J is the Landé gyromagnetic factor ($g_J = 2.274$), μ_B is the Bohr magneton, and J is the system's spin. The magnetization is readily written as follows:

$$M = N g_J \mu_B J B_J(J, y). \quad (2)$$

The magnetic susceptibility is computed by $\chi = (\partial M / \partial B)_{B=0}$. Figure 2 depicts the Brillouin magnetic susceptibility as a function of temperature under various magnetic fields. Remarkably, at low T for a vanishing magnetic field, χ diverges as it occurs for a magnetic field-induced QCP. It turns out that, for real systems, magnetic moments are always interacting. Such interaction is rather small when compared with the thermal energy $k_B T$, but it becomes relevant at low T and, thus, a long-range magnetic ordering takes place [41]. The calculation of the MCE for the Brillouin paramagnet is straightforward. For arbitrary values of J, it can be calculated using the expression [3],

$$\Gamma_{\mathrm{mag}} = -\frac{1}{T}\frac{(\partial S/\partial B)_T}{(\partial S/\partial T)_B}. \quad (3)$$

We can calculate the entropy S employing the Helmholtz free-energy F per spin,
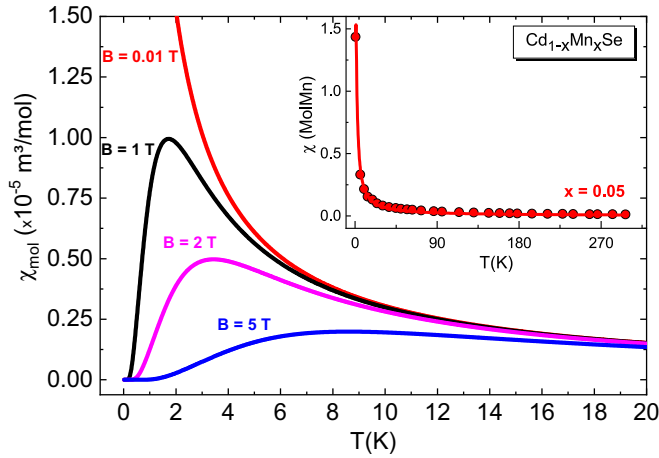
$$F = -k_B T \ln[Z_J(y)], \quad (4)$$

FIG. 2. Main panel: molar magnetic susceptibility $\chi_{\mathrm{mol}} = \mu_0(dM/dB)$ as a function of T at various magnetic fields for the Brillouin paramagnet employing $J = 3/2$. The inset: experimental data of the magnetic susceptibility χ as a function of temperature for the $Cd_{1-x}Mn_xSe$ paramagnetic system with 5% concentration of Mn ($x = 0.05$) under a magnetic field of 8.5 kOe. The low- and high-temperature data were taken after zero-field cooling for increasing T (5 K $\leqslant T \leqslant$ 35 K) and after field cooling of decreasing T, respectively. The red solid line represents a Curie-like fitting, employing the values of g and J of the $Cd_{1-x}Mn_xSe$ system. The obtained number of spins in the system is $N \sim (3 \times 10^{22})$. Data taken from Fig. 1 of Ref. [42]. Further details are discussed in the main text.

where $Z_J(y)$ is the partition function, given by

$$Z_J(y) = \frac{\sinh\left[(2J+1)\frac{y}{2J}\right]}{\sinh\left[\frac{y}{2J}\right]}. \tag{5}$$

Thus, the Helmholtz free energy is as follows:

$$F = -k_B T \ln\left(\frac{\sinh\left[\frac{(2J+1)y}{2J}\right]}{\sinh\left[\frac{y}{2J}\right]}\right). \tag{6}$$

From Eq. (6), the entropy S can be easily calculated

$$S = -\left(\frac{\partial F}{\partial T}\right)_B. \tag{7}$$

The resulting expression for the entropy reads

$$S(y) = k_B[\ln Z_J(y) - y B_J(y)]. \tag{8}$$

Regarding the entropy (S) [Eq. (8)], it is worth recalling the adiabatic demagnetization using a paramagnetic system. Upon applying a magnetic field, the spins are aligned in the direction of B reducing, thus, the entropy of the system. Then, the magnetic field is removed adiabatically, and the temperature of the system decreases. Such a well-known adiabatic demagnetization procedure is frequently employed in order to achieve low temperatures in the microkelvin range.

The calculation of the MCE is straightforward, and the resulting expression for any J regarding the Brillouin paramagnet reads
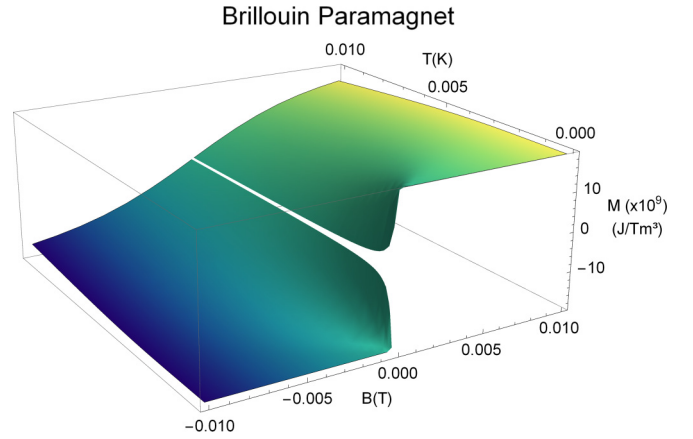
$$\Gamma_{\mathrm{mag}} = \frac{1}{B}. \tag{9}$$

FIG. 3. Magnetization M as a function of temperature ($0 < T < 0.01$ K) and magnetic-field (-0.01 T $< B < 0.01$ T) for the classical Brillouin paramagnet.

From Eq. (9), one can again directly conclude that Γ_{mag} for the Brillouin paramagnet depends only on the magnetic field, and it diverges as $B \to 0$ at any temperature (see Fig. 3).

The effect of the SO interaction on Γ_{mag} is discussed in the next section.

III. THE SPIN-ORBIT INTERACTION

The interaction between the orbital angular momentum of the nucleus and the electron spin angular momentum is the well-known SO interaction [31]. The latter leads to a splitting of the electrons' energy levels in an atom. Since the energy levels are affected by the SO interaction, it is of our interest to study the influence of the SO interaction on the Grüneisen parameter. Thus, in order to take into account the SO interaction, it is necessary to make use of the Hamiltonian, which considers such interaction. For a $S = 3/2$ system, such a Hamiltonian was already reported in Refs. [43–45], and it has the form

$$H_{\mathrm{spin}} = \mu_B g_{pa} B_z S_z + \mu_B g_{pe}(B_x S_x + B_y S_y) + D S_z^2, \tag{10}$$

where g_{pa}, g_{pe}, and D stand for the gyromagnetic factors of the anisotropic system and the zero-field splitting constant [$D = (5.479 \times 10^{-23})$ J $= 3.97$ K], respectively. The matrices S_x, S_y, and S_z can be easily found by the usual operation rules of quantum mechanics. Thus, it is only necessary to diagonalize the resulting operator H_{spin} in order to obtain the eigenenergies. Considering that $B_y = B_z = 0$ and $B_x \neq 0$ as reported in Ref. [45], one obtains

$$H_{\mathrm{spin}} = \begin{pmatrix} \frac{9\hbar^2 D}{4} & \frac{\sqrt{3}\hbar\mu_B g_{pe} B_x}{2} & 0 & 0 \\ \frac{\sqrt{3}\hbar\mu_B g_{pe} B_x}{2} & \frac{\hbar^2 D}{4} & \hbar\mu_B g_{pe} B_x & 0 \\ 0 & \hbar\mu_B g_{pe} B_x & \frac{\hbar^2 D}{4} & \frac{\sqrt{3}\hbar\mu_B g_{pe} B_x}{2} \\ 0 & 0 & \frac{\sqrt{3}\hbar\mu_B g_{pe} B_x}{2} & \frac{9\hbar^2 D}{4} \end{pmatrix},$$

and the diagonalization yields four values of eigenenergies given by

$$E_1 = \tfrac{1}{2}\mu_B g_{pe} B_x + \tfrac{5}{4}D + \sqrt{\mu_B^2 g_{pe}^2 B_x^2 - D g_{pe}\mu_B B_x + D^2},$$

$$E_2 = \tfrac{1}{2}\mu_B g_{pe} B_x + \tfrac{5}{4}D - \sqrt{\mu_B^2 g_{pe}^2 B_x^2 - D g_{pe}\mu_B B_x + D^2},$$

$$E_3 = -\tfrac{1}{2}\mu_B g_{pe} B_x + \tfrac{5}{4}D + \sqrt{\mu_B^2 g_{pe}^2 B_x^2 + D g_{pe}\mu_B B_x + D^2},$$

$$E_4 = -\tfrac{1}{2}\mu_B g_{pe} B_x + \tfrac{5}{4}D - \sqrt{\mu_B^2 g_{pe}^2 B_x^2 + D g_{pe}\mu_B B_x + D^2}.$$

$$(11)$$

Yet, the free energy for the Brillouin-like paramagnet considering the SO interaction reads

$$
\begin{aligned}
F = -k_B T \ln\Bigg\{ & 2\exp\left(-\frac{2Bg_J\mu_B + 5D}{4k_B T}\right) \\
& \times \left[\cosh\left(\frac{\sqrt{B^2 g_J^2 \mu_B^2 - BD g_J \mu_B + D^2}}{k_B T}\right)\right. \\
& + \exp\left(\frac{Bg_J\mu_B}{k_B T}\right) \\
& \left.\times \cosh\left(\frac{\sqrt{B^2 g_J^2 \mu_B^2 + BD g_J \mu_B + D^2}}{k_B T}\right)\right]\Bigg\}.
\end{aligned}
$$

$$(12)$$

Replacing $D = 0$ in Eq. (12) and simplifying the resultant expression, it is possible to obtain

$$F = -k_B T \ln\left[4\cosh\left(\frac{y}{2J}\right)\cosh\left(\frac{y}{J}\right)\right].$$

Employing the hyperbolic trigonometric identities and again simplifying the equation,

$$F = -k_B T \ln\left(\frac{\sinh\left[\frac{2y}{J}\right]}{\sinh\left[\frac{y}{2J}\right]}\right), \qquad (13)$$

which is the very same free energy of the Brillouin paramagnet in Eq. (6) employing $J = 3/2$ without considering the SO interaction. In other words, the classical Brillouin paramagnet is recovered when the zero-field splitting $D \to 0$. Since the eigenenergies were found, it is then possible to obtain the partition function and, consequently, the observable quantities, especially the magnetic Grüneisen parameter $\Gamma_{\rm mag}$ (see the Appendix). In this context, we have performed numerical calculations and made the density and three-dimensional plots of both the magnetization and the magnetic Grüneisen parameter for the Brillouin paramagnet as well as considering the SO interaction. As can be seen from Fig. 4, a comparison between the classical Brillouin system for $S = 3/2$ and SO coupling shows that the magnetization density plot is slightly altered for nonzero D. Figure 4 shows that the magnetization is much more sensitive to magnetic-field changes for any value of temperature in the case of SO interaction. The dashed white lines in the density plots of Fig. 4 were inserted aiming to compare the enhancement of $\Gamma_{\rm mag}$ for T and $B \to 0$ (magnetization cone) and its narrowing when SO interactions
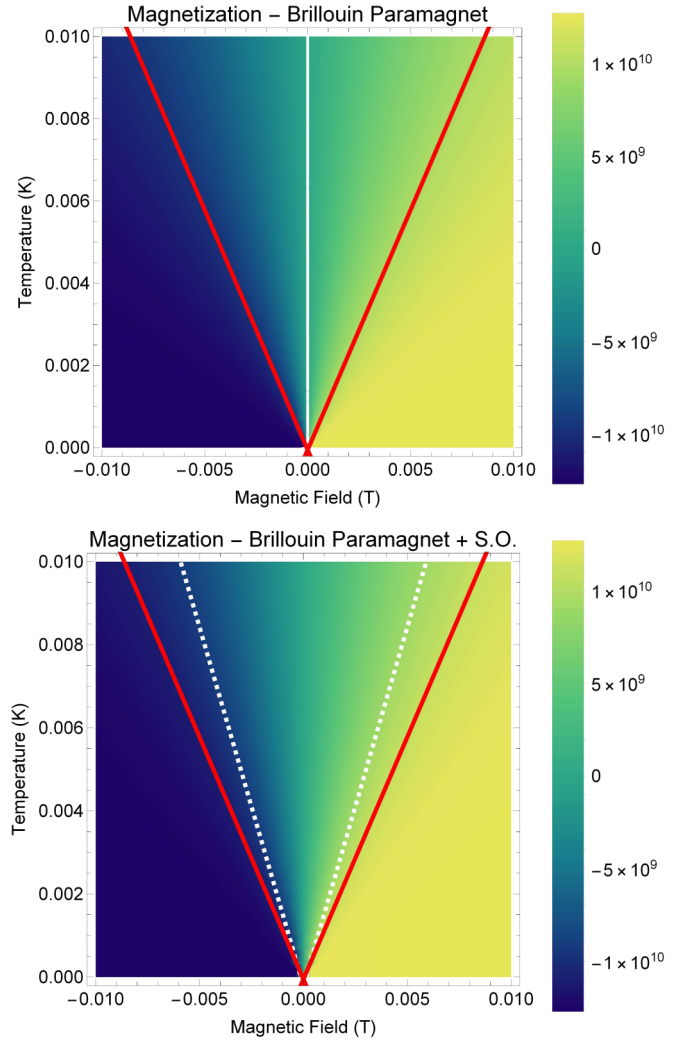

FIG. 4. Density plots of the magnetization as a function of magnetic-field (-0.01 T $< B < 0.01$ T) and temperature ($T < 0.01$ K) for a Brillouin paramagnet with (lower panel) and without (upper panel) considering the SO interaction. The solid red (upper and lower panels) and dashed white (lower panel) lines are guides to the eyes. Details in the main text.

are taken into account. Note that, in the lower panel of Fig. 4, the red solid line (without SO) is plotted together with the white dashed line (considering SO) for a proper comparison. Thus, it is clear that the angular coefficient of the lines is changed when SO interaction is considered, narrowing the magnetization cone. For the case where the SO interaction is lacking, the magnetization presents a weaker dependence regarding magnetic-field changes. From the eigenenergies, we can see that, as the magnetic field approaches zero, the degree of degeneracy of the eigenenergies is two, whereas, for the case where no SO interaction is considered (analogously, for $D = 0$), we have a degree of degeneracy four (all the eigenenergies have the same value and equal zero) (see Fig. 5). The magnetic Grüneisen parameter presents a singular behavior in the vicinity of $T = 0$ K and $B = 0$ T (Fig. 6). In other words, $\Gamma_{\rm mag}$ diverges as $B \to 0$ T, resembling a fingerprint of a quantum phase transition. At this point, it is important to recall the results reported in Ref. [3] obtained using scaling
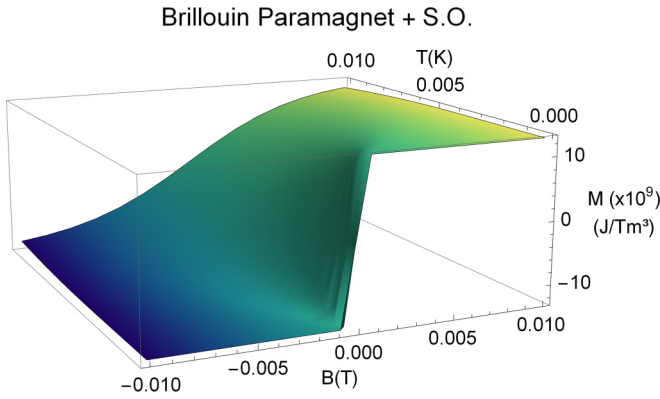
FIG. 5. Magnetization M as a function of temperature ($0 < T < 0.01$ K) and magnetic-field (-0.01 T $< B < 0.01$ T) for the Brillouin paramagnet considering SO interaction. Details in the main text.

arguments for any QCP tuned by a magnetic field,

$$\Gamma_{B,cr}(T \to 0) = -G \frac{1}{(B - B_c)}, \tag{14}$$

where cr refers to the critical contribution of Γ_B, B_c is the critical magnetic field and G is a universal prefactor. Note that Eqs. (14) and (9) are quite similar. The presence of an additional pseudoenergy scale, namely, D gives rise to a temperature-dependent magnetic Grüneisen parameter (cf. Fig. 6), and it diverges upon approaching $B = 0$ T and $T = 0$ K.

IV. THE ONE-DIMENSIONAL ISING MODEL UNDER A LONGITUDINAL FIELD

For the 1DI model, all the physical quantities discussed in this section are given per mole of particles. For the sake of completeness, we start recalling the 1DI model and its key equations [31] where the Hamiltonian for a linear chain of N
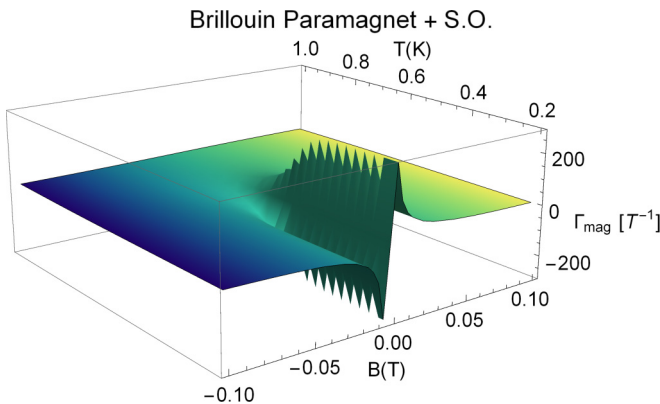

FIG. 6. Three-dimensional plot of the magnetic Grüneisen parameter Γ_{mag} as a function of magnetic field and temperature for the Brillouin paramagnet considering the SO interaction. The depicted *zigzag* is a consequence of the numerical calculation and, thus, not intrinsic.

spins is expressed by the form

$$H = \sum_{i=1}^{N} J_{i,i+1} S_i S_{i+1} - B \sum_{i=1}^{N} S_i, \tag{15}$$

where $J_{i,i+1}$ is the coupling constant between the ith and the $i + 1$ sites and S_i refers to the spin of the ith site. Nevertheless, the S_i terms are normalized to unity so that we can analyze the energy scales and the coupling term without adding numerical constant contributions. Also, the magnetization is given by

$$M_{1DI}(T, B) = \mu_B \frac{\sinh(\beta \mu_B B)}{[\cosh^2(\beta \mu_B B) - 2e^{2\beta J} \sinh(2\beta J)]^{1/2}}, \tag{16}$$

where $\beta = 1/k_B T$ and J is the coupling constant between two neighbor spins. From Eq. (16), one can deduce that, for the 1DI model, spontaneous magnetization is not possible, namely, $M(T \neq 0, B = 0) = 0$. It is now worth analyzing the 1DI magnetic susceptibility, which reads [31]

$$\chi_{1DI}(T, B) = \beta \mu_B^2 \frac{\cosh(\beta \mu_B B)[1 - 2e^{-2\beta J} \sinh(2\beta J)]}{[\cosh^2(\beta \mu_B B) - 2e^{-2\beta J} \sinh(2\beta J)]^{3/2}}. \tag{17}$$

For vanishing magnetic-field $\chi(T, B \to 0) = \beta \mu_B^2 e^{2\beta J}$, i.e., for $B \to 0$ and $T \to 0$, χ diverges as expected for a QCP. In other words, for the 1DI model at $T = 0$ K, a vanishing small external magnetic field suffices to produce long-range magnetic ordering. The specific heat at zero field is given by

$$C_{B=0 \text{ T}} = k_B \frac{\beta^2 J^2}{\cosh^2(\beta J)}. \tag{18}$$

In order to perform an analysis of the 1DI model for generic B and T, the Helmholtz free energy is calculated employing the expression [1],

$$F(B, T) = -J - k_B T \ln[\eta + \sqrt{\tau^2 + \vartheta}], \tag{19}$$

where η, τ, and ϑ stand for

$$\vartheta = \exp\left(\frac{-4J}{k_B T}\right); \quad \eta = \cosh\left(\frac{\mu_B B}{k_B T}\right); \quad \tau = \sinh\left(\frac{\mu_B B}{k_B T}\right). \tag{20}$$

Figure 7 shows the behavior of the free energy for different applied magnetic fields as a function of temperature. It can be seen that, if both J and B are held constant, an increase in the temperature causes a decrease in the free energy. We also introduce an equivalent definition of the MCE via Maxwell relations, namely, the magnetic Grüneisen parameter [19],

$$\Gamma_{mag} = -\frac{(\partial M / \partial T)_B}{C_B}, \tag{21}$$

where

$$C_B = T \left(\frac{\partial S}{\partial T}\right)_B. \tag{22}$$

Since the magnetization was already presented, the calculation of Γ_{mag} and the obtainment of the MCE for the 1DI model under a longitudinal field is also straightforward. From Eq. (16), we can see that, as $B \to 0$, also $M \to 0$, which means that there is no spontaneous magnetization at finite
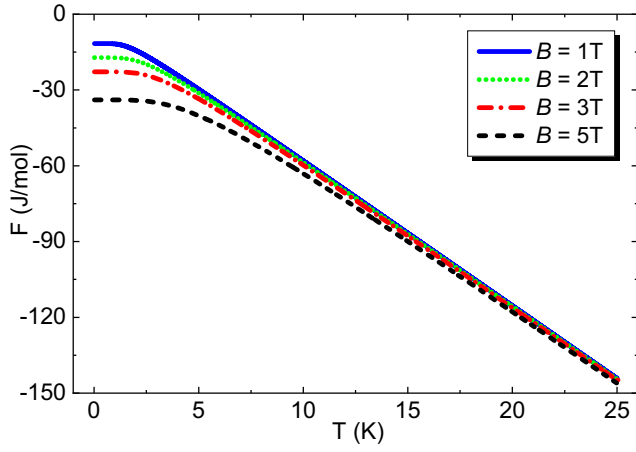
FIG. 7. The Helmholtz free-energy F [Eq. (19)] as a function of temperature for various magnetic fields, cf. label. From the data, it can be seen that, as the temperature increases, the free energy decreases. Further details in the main text.

temperature for the 1DI model as previously stated. Figures 8 and 9 show the behavior of the magnetization when T is held constant and B varies and when B is held constant and T varies, respectively. It is possible already to detect the absence of long-range magnetic order in the system. The Mermin-Wagner theorem ensures that, for the 1DI model, the spontaneous magnetization is zero for any finite temperature value. If the system would present spontaneous magnetization, in Fig. 8 it would be possible to see a discontinuity in the magnetization at $B = 0$ for a certain range of temperature values, given by $T < T_c$, which would be characteristic of a phase transition from ferromagnetic to paramagnetic behavior. However, this behavior is not present in the 1DI model. Thus, we can calculate analytically the Grüneisen parameter. The derivatives can be performed straightforwardly yielding

$$S = k_B \left[\frac{\Sigma}{k_B T (\sqrt{\vartheta + \tau^2} + \eta)} + \ln(\sqrt{\vartheta + \tau^2} + \eta) \right], \quad (23)$$
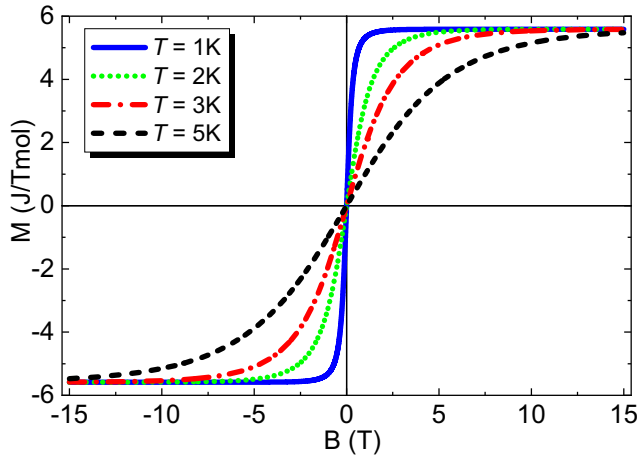

FIG. 8. Magnetization M as a function of magnetic-field B at various temperatures as indicated in the label. Further details are given in the main text.
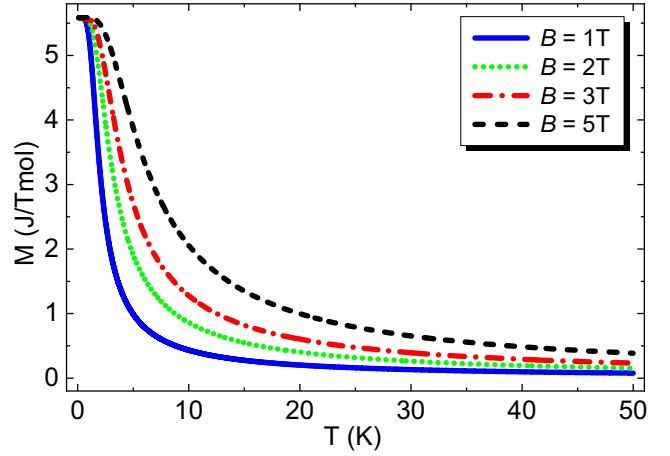

FIG. 9. Magnetization M as a function of temperature T under various values of magnetic field as indicated in the label. Further details are given in the main text.

$$\left(\frac{\partial M}{\partial T} \right)_B = -\frac{2J\tau + B\eta}{T^2 \sqrt{\vartheta + \tau^2}(k_B \vartheta^{-1}\tau^2 + k_B)}, \quad (24)$$

$$C_B = \left[\frac{\Sigma}{T(\sqrt{\vartheta + \tau^2} + \eta)} \right] + \frac{T\Upsilon}{\Phi\varsigma} - \frac{\Theta T\Sigma}{\varsigma^2}, \quad (25)$$

where the additional parameters Υ, Φ, Θ, ς, and Σ were introduced purely for compactness as follows:

$$\Upsilon = 16J^2\tau^2 + 8J^2\vartheta - \frac{1}{2}D^2\vartheta^{-1}\sinh^2\left(\frac{2\mu_B B}{k_B T} \right)$$

$$+ D^2\vartheta^{-1}\tau \sinh\left(\frac{2\mu_B B}{k_B T} \right)\sqrt{\vartheta + \tau^2}$$

$$+ 2B^2 \cosh\left(\frac{2\mu_B B}{k_B T} \right)(\vartheta^{-1}\tau^2 + 1)$$

$$+ 2B^2\eta\sqrt{\vartheta + \tau^2} + 4JB \sinh\left(\frac{2\mu_B B}{k_B T} \right), \quad (26)$$

$$\Phi = 2T^2\sqrt{\vartheta + \tau^2}(k_B\vartheta^{-1}\tau^2 + k_B), \quad (27)$$

$$\Theta = \frac{2\epsilon\vartheta - \frac{1}{2}B\sinh\left(\frac{2\mu_B B}{k_B T} \right)}{k_B T\sqrt{\vartheta + \tau^2}} + \sqrt{\vartheta + \tau^2} - \frac{B\tau}{k_B T^2}, \quad (28)$$

$$\varsigma = T(\sqrt{\vartheta + \tau^2} + \eta), \quad (29)$$

$$\Sigma = \frac{\vartheta\left[2J - \frac{1}{2}B\vartheta^{-1}\sinh\left(\frac{2\mu_B B}{k_B T} \right) \right]}{\sqrt{\vartheta + \tau^2}} - D\tau. \quad (30)$$

It can be seen that the MCE for the 1DI model is far from trivial and we study its behavior by maintaining B and J constant and varying the temperature, cf. Fig. 10. Thus, Γ_{mag} for the 1DI model is given by the expression,

$$\Gamma_{mag} = \frac{\frac{2J\tau + B\eta}{T^2\sqrt{\vartheta + \tau^2}(k_B\vartheta^{-1}\tau^2 + k_B)}}{\left[\frac{\Sigma}{T(\sqrt{\vartheta + \tau^2} + \eta)} \right] + \frac{T\Upsilon}{\Phi\varsigma} - \frac{T\Theta\Sigma}{\varsigma^2}}. \quad (31)$$

It is possible to make a Taylor series expansion for Γ_{mag} for the case of the 1DI model around $B = 0$ for a fixed temperature
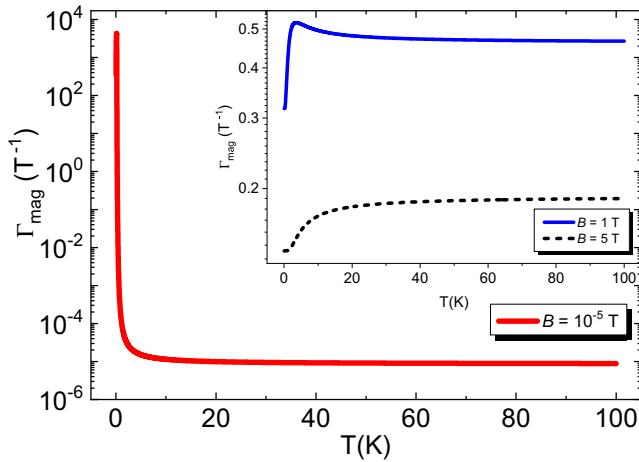
FIG. 10. Main panel: the magnetic Grüneisen parameter Γ_{mag} versus T under low-field ($B = 10^{-5}$ T). Note the logarithmic scale. As $T \to 0$ K, Γ_{mag} diverges. The absence of a classical phase transition at finite temperatures can be interpreted as a direct consequence of the Mermin-Wagner theorem. The inset: Γ_{mag} versus T for $B = 1$ and 5 T. Further details in the main text.

T (see Fig. 11). The obtained expression reads

$$\Gamma_{\mathrm{mag}}(B, T) = \left[\frac{(e^{2J/k_B T} + 1)^2 \mu_B^2 (2J + k_B T)}{4J^2 k_B T} \right] B + O(B^3),$$
(32)

where $O(B^3)$ represents the higher-order terms in the expansion. For $T \to 0$ K, Γ_{mag} diverges, and a discontinuity takes place at $T = 0$ K and $B = 0$ T, cf. Fig. 12. From Eq. (32), it is shown that the mathematical function describing Γ_{mag} for the 1DI model is odd with respect to the magnetic-field
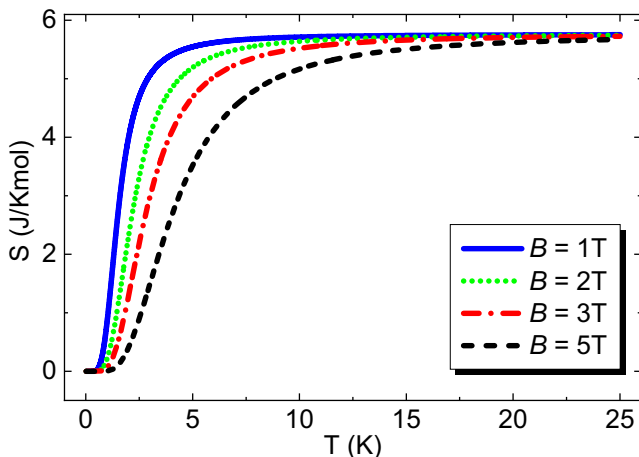

FIG. 11. Entropy S as a function of temperature T for various values of magnetic-field B, cf. indicated in the label. It can be seen that the entropy increases with temperature, which is the expected behavior of the system, i.e., the magnetic disorder is increased upon increasing the thermal energy. Another interesting aspect of the entropy function is its saturation point. When the temperature is sufficiently increased, the entropy reaches a constant value. The required temperature to the saturation increases as the magnetic coupling constant J is increased.
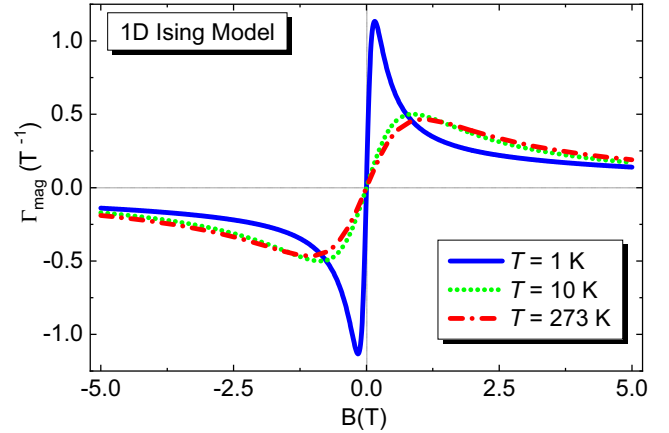

FIG. 12. The magnetic Grüneisen parameter Γ_{mag} as a function of the magnetic-field B for various temperatures (see the label) for the 1DI model under the longitudinal field. By tuning B between positive and negative values, Γ_{mag} changes sign.

B. Hence, Eq. (32) also explains the obtained symmetrical behavior of Γ_{mag} upon varying the magnetic-field B from negative to positive values, cf. Fig. 12. In order to analytically demonstrate the asymptotic equivalence of Γ_{mag} for the 1DI and the Brillouin model, it is possible to make a change in the temperature variable T to $1/T$ and make an expansion in a Taylor series around $1/T \to 0$ [46]. Thus, the expression of Γ_{mag} for the 1DI model is simplified and is expressed by

$$\Gamma_{\mathrm{mag}}(B, T \to \infty) = \frac{\mu_B^2 B}{J^2 + \mu_B^2 B^2}.$$
(33)

In this context, when $J = 0$, the Γ_{mag} for the Brillouin model is elegantly recovered, namely, $1/B$ [Eq. (9)]. This means that, at high temperatures, and upon neglecting the magnetic coupling between the nearest-neighbor spins, we have shown analytically that the two magnetic models are equivalent. Similarly, it is possible to make the very same expansion for Γ_{mag} in the case of the Brillouin model upon considering the SO interaction,

$$\Gamma_{\mathrm{mag}}(B, T \to \infty) = \frac{5g_J^2 \mu_B^2 B}{4D^2 + 5g_J^2 \mu_B^2 B^2}.$$
(34)

Upon comparing Eqs. (33) and (34), it is clear that both expressions have the same mathematical structure except for the constant term J^2. Making $J = \sqrt{4/5}D/g_J$ and replacing it in Eq. (33), it can be shown that the two models are also equivalent in the asymptotic regime, namely, for $1/T \to 0$. Such mathematical similarity in the regime of high temperatures is a direct consequence of the dominant effects from thermal fluctuations, and, obviously, this does not mean that the models are physically equivalent. Yet, still considering Eq. (34), it is clear that for $D \to 0$, Eq. (9) is nicely restored. Summarizing the results obtained for the longitudinal 1DI model: (i) It does not present any classical critical behavior for any finite value of temperature as a consequence of the Mermin-Wagner theorem, and (ii) for $T \to 0$ K, it is tempting to say that the system shows intrinsic quantum critical behavior. It is important to emphasize that the Grüneisen

parameter cannot be calculated at T exactly equal to 0 K since the corresponding function is not determined at this point.

V. CONCLUDING REMARKS

Grüneisen, in 1908, realized that the volume dependence of the vibrational energy must be taken into account in order to explain thermal expansion. Slowly but steadily, the Grüneisen parameter has been incorporated as a thermodynamic coefficient, both in thermodynamical textbooks and in experimental physics; and when measured, it can provide information on other thermodynamic coefficients as shown in Refs. [28,47]. As a second step from our previous work [28], we have considered the magnetic analog of the Grüneisen parameter as a tool to further probe magnetic systems, in particular, at low temperatures when quantum phase transitions are relevant. In the Introduction, we mentioned several exotic manifestations of matter where the Grüneisen parameter could be measured. Following the Introduction, we computed this parameter for several known theoretical models, namely, the Brillouin paramagnet, yielding a temperature-independent Grüneisen parameter, proportional to the inverse of the applied magnetic field; SO interaction model yields a diverging Grüneisen parameter as the temperature goes to zero; and the longitudinal 1D Ising model, known not to exhibit any kind of phase transition at finite temperature as a consequence of the well-known Mermin-Wagner theorem. Also, we did find an equivalence at high temperatures between the 1D Ising model with a Brillouin paramagnet with vanishing coupling constant J and with or without a SO interaction included on the latter. Thus, the magnetic Grüneisen parameter can be seen as a smoking gun when we probe critical points. The relevance

of the mutual interactions for an ideal paramagnet in the limit B and $T \rightarrow 0$ was briefly discussed. Future work will consider other systems where the thermodynamic coefficients are not readily computed in a complete analytic fashion.

APPENDIX

For the Brillouin-like paramagnet considering SO interaction, the magnetic Grüneisen parameter Γ_{mag} reads

$$\Gamma_{\mathrm{mag}} = \frac{a(T, B)}{c(T, B)}, \tag{A1}$$

where

$$
\begin{aligned}
a(T, B) = &-g_J\mu_B\big[\sinh[A]\{F(2D^2 - 3BDg_J\mu_B + 4B^2g_J{}^2\mu_B{}^2)\cosh[C] + 2Bg_J\mu_B(D^2 + 2B^2g_J{}^2\mu_B{}^2)\sinh[C]\} \\
&- G\cosh[A](2D^2\sinh[C] + Bg_J\mu_B\{6F\cosh[C] + (3D + 4Bg_J\mu_B)\sinh[C]\}) \\
&- 2FG\{2Bg_J\mu_B\cosh[(Bg_J\mu_B)/(k_BT)] + D\sinh[(Bg_J\mu_B)/(k_BT)]\}\big], \\
c(T, B) = &\,2FG\big(\cosh[A]\{(2D^2 + 3B^2g_J{}^2\mu_B{}^2)\cosh[C] + 2BFg_J\mu_B\sinh[C]\} + 2\{(D^2 + B^2g_J{}^2\mu_B{}^2)\cosh[(Bg_J\mu_B)/(k_BT)] \\
&- G\sinh[A](Bg_J\mu_B\cosh[C] + F\sinh[C]) + BDg_J\mu_B\sinh[(Bg_J\mu_B)/(k_BT)]\}\big), \\
A = &\,\frac{\sqrt{B^2g_J{}^2\mu_B{}^2 - Bg_J\mu_BD + D^2}}{k_BT}, \\
C = &\,\frac{\sqrt{B^2g_J{}^2\mu_B{}^2 + Bg_J\mu_BD + D^2}}{k_BT}, \\
F = &\,\sqrt{B^2g_J{}^2\mu_B{}^2 + Bg_J\mu_BD + D^2}, \\
G = &\,\sqrt{B^2g_J{}^2\mu_B{}^2 - Bg_J\mu_BD + D^2}.
\end{aligned}
$$

[1] K. Huang, *Statistical Mechanics* (Wiley, New York, 1987).

[2] S. Sachdev, *Quantum Phase Transitions* (Cambridge University Press, Cambridge, U.K., 2001).

[3] L. Zhu, M. Garst, A. Rosch, and Q. Si, Universally Diverging Grüneisen Parameter and the Magnetocaloric Effect Close to Quantum Critical Points, Phys. Rev. Lett. **91**, 066404 (2003).

[4] R. Küchler, N. Oeschler, P. Gegenwart, T. Cichorek, K. Neumaier, O. Tegus, C. Geibel, J. A. Mydosh, F. Steglich, L. Zhu, and Q. Si, Divergence of the Grüneisen Ratio at Quantum Critical Points in Heavy Fermion Metals, Phys. Rev. Lett. **91**, 066405 (2003).

[5] A. Steppke, R. Küchler, S. Lausberg, E. Lengyel, L. Steinke, R. Borth, T. Lhmann, C. Krellner, M. Nicklas, C. Geibel,

F. Steglich, and M. Brando, Ferromagnetic quantum critical point in the heavy-fermion metal YbNi$_4$(P$_{1-x}$As$_x$)$_2$, Science **339**, 933 (2013).

[6] S. Paschen, T. Luhmann, S. Wirth, P. Gegenwart, O. Trovarelli, C. Geibel, F. Steglich, P. Coleman, and Q. Si, Hall-effect evolution across a heavy-fermion quantum critical point, Nature (London) **432**, 881 (2004).

[7] H. V. Löhneysen, A. Rosch, M. Vojta, and P. Wölfle, Fermi-liquid instabilities at magnetic quantum phase transitions, Rev. Mod. Phys. **79**, 1015 (2007).

[8] S. Kambe, H. Sakai, Y. Tokunaga, G. Lapertot, T. D. Matsuda, G. Knebel, J. Flouquet, and R. E. Walstedt, Degenerate Fermi and non-Fermi liquids near a quantum critical phase transition, Nat. Phys. **10**, 840 (2011).

[9] M. A. Tanatar, J. Paglione, C. Petrovic, and L. Taillefer, Anisotropic violation of the Wiedemann-Franz law at a quantum critical point, Science **316**, 1320 (2007).

[10] M. Klanjšek, A critical test of quantum criticality, Physics **7**, 74 (2014).

[11] P. Gegenwart, Q. Si, and F. Steglich, Quantum criticality in heavy-fermion metals, Nat. Phys. **4**, 186 (2008).

[12] L. Squillante *et al.* (unpublished).

[13] M. E. Zhitomirsky and A. Honecker, Magnetocaloric effect in one-dimensional antiferromagnets, J. Stat. Mech.: Theory Exp. (2004) P07012.

[14] A. W. Kinross, M. Fu, T. J. Munsie, H. A. Dabkowska, G. M. Luke, Subir Sachdev, and T. Imai, Evolution of Quantum Fluctuations Near the Quantum Critical Point of the Transverse Field Ising Chain System CoNb$_2$O$_6$, Phys. Rev. X **4**, 031008 (2014).

[15] L. Savary, E.-G. Moon, and L. Balents, New Type of Quantum Criticality in the Pyrochlore Iridates, Phys. Rev. X **4**, 041027 (2014).

[16] L. Mittelstädt, M. Schmidt, Z. Wang, F. Mayr, V. Tsurkan, P. Lukenheimer, D. Ish, L. Balents, J. Deisenhofer, and A. Loidl, Spin-orbiton and quantum criticality in FeSc$_2$S$_4$, Phys. Rev. B **91**, 125112 (2015).

[17] F. A. Dessotti, L. S. Ricco, Y. Marques, L. H. Guessi, M. Yoshida, M. S. Figueira, M. de Souza, Pasquale Sodano, and A. C. Seridonio, Unveiling Majorana quasiparticles by a quantum phase transition: Proposal of a current switch, Phys. Rev. B **94**, 125426 (2016).

[18] Y. Matsumoto, S. Nakatsuji, K. Kuga, Y. Karaki, N. Horie, Y. Shimura, T. Sakakibara, A. H. Nevidomskyy, and P. Coleman, Quantum criticality without tuning in the mixed valence compound β-YbAlB$_4$, Science **331**, 316 (2011).

[19] M. Garst and A. Rosch, Sign change of the Grüneisen parameter and magnetocaloric effect near quantum critical points, Phys. Rev. B **72**, 205129 (2005).

[20] Y. Tokiwa, T. Radu, C. Geibel, F. Steglich, and P. Gegenwart, Divergence of the Magnetic Grüneisen Ratio at the Field-Induced Quantum Critical Point in YbRh$_2$Si$_2$, Phys. Rev. Lett. **102**, 066401 (2009).

[21] N. A. Fortune, S. T. Hannahs, Y. Yoshida, T. E. Sherline, T. Ono, H. Tanaka, and Y. Takano, Cascade of Magnetic-Field-Induced Quantum Phase Transitions in a Spin-$\frac{1}{2}$ Triangular-Lattice Antiferromagnet, Phys. Rev. Lett. **102**, 257201 (2009).

[22] S. Zaum, K. Grube, R. Schäfer, E. D. Bauer, J. D. Thompson, and H. v. Löhneysen, Towards the Identification of a Quantum Critical Line in the (*p*, *b*) Phase Diagram of CeCoIn$_5$ with Thermal-Expansion Measurements, Phys. Rev. Lett. **106**, 087003 (2011).

[23] Y. Tokiwa, E. D. Bauer, and P. Gegenwart, Zero-Field Quantum Critical Point in CeCoIn$_5$, Phys. Rev. Lett. **111**, 107003 (2013).

[24] K. Deguchi, S. Matsukawa, N. K. Sato, T. Hattori, K. Ishida, H. Takakura, and T. Ishimasa, Quantum critical state in a magnetic quasicrystal, Nat. Mater. **11**, 1013 (2012).

[25] M. de Souza, A. Brühl, C. Strack, B. Wolf, D. Schweitzer, and M. Lang, Anomalous Lattice Response at the Mott Transition in a Quasi-2D Organic Conductor, Phys. Rev. Lett. **99**, 037003 (2007).

[26] L. Bartosch, M. de Souza, and M. Lang, Scaling Theory of the Mott Transition and Breakdown of the Grüneisen Scaling Near a Finite-Temperature Critical End Point, Phys. Rev. Lett. **104**, 245701 (2010).

[27] M. de Souza and L. Bartosch, Probing the Mott physics in κ-(BEDT-TTF)$_2$X salts via thermal expansion, J. Phys.: Condens. Matter **27**, 053203 (2015).

[28] M. de Souza, P. Menegasso, R. Paupitz, A. Seridonio, and R. E Lagos, Grüneisen parameter for gases and superfluid helium, Eur. J. Phys. **37**, 055105 (2016).

[29] D. Bitko, T. F. Rosenbaum, and G. Aeppli, Quantum Critical Behavior for a Model Magnet, Phys. Rev. Lett. **77**, 940 (1996).

[30] J. Steinberg, N. P. Armitage, F. Essler, and S. Sachdev, NMR relaxation in Ising spin chains, Phys. Rev. B **99**, 035156 (2019).

[31] W. Nolting and A. Ramakanth, *Quantum Theory of Magnetism* (Springer, Berlin, Heidelberg, 2009).

[32] N. D. Mermin and H. Wagner, Abscence of Ferromagnetism or Antiferromagnetism in One- or Two-Dimensional Isotropic Heinsenberg Models, Phys. Rev. Lett. **17**, 1133 (1966).

[33] J. Zhang, F. M. Cucchietti, C. M. Chandrashekar, M. Laforest, C. A. Ryan, M. Ditty, A. Hubbard, J. K. Gamble, and R. Laamme, Direct observation of quantum criticality in Ising spin chains, Phys. Rev. A **79**, 012305 (2009).

[34] F. Franchini, J. Cui, L. Amico, H. Fan, M. Gu, V. Korepin, L. C. Kwek, and V. Vedral, Local Convertibility and the Quantum Simulation of Edge States in Many-Body Systems, Phys. Rev. X **4**, 041028 (2014).

[35] P. Gegenwart, Classification of materials with divergent magnetic Grüneisen parameter, Philos. Mag. **97**, 3415 (2017).

[36] R. Baierlein, *Thermal Physics* (Cambridge University Press, Cambridge, U.K., 1999).

[37] L. Onsager, Crystal statistics. I. A two-dimensional model with an order-disorder transition, Phys. Rev. **65**, 117 (1944).

[38] J. Strečka, H. Čenčariková, and M. Jaščur, Exact results of the one-dimensional transverse Ising model in an external longitudinal magnetic field, Acta Electrotechnica et Informatica **2**, 107 (2002).

[39] R. J. Baxter, *Exactly Solved Models in Statistical Mechanics* (Dover, Mineola, NY, 1982).

[40] R. K. Pathria, *Statistical Mechanics*, second ed. (Butterworth-Heinemann, Oxford, 1996).

[41] C. B. P. Finn, *Thermal Physics*, second ed., Physics and Its Applications (Taylor & Francis, Boca Raton, FL, 1993).

[42] S. B. Oseroff, Magnetic susceptibility and EPR measurements in concentrated spin-glasses: Cd$_{1-x}$Mn$_x$Te and Cd$_{1-x}$Mn$_x$Se, Phys. Rev. B **25**, 6584 (1982).

[43] P. Koidl, Optical absorption of Co^{2+} in ZnO, Phys. Rev. B **15**, 2493 (1977).

[44] P. Sati, R. Hayn, R. Kuzian, S. Regnier, S. Schäfer, A. Stepanov, C. Morhain, C. Deparis, M. Laügt, M. Goiran, and Z. Golacki, Magnetic Anisotropy of Co^{2+} as Signature of Intrinsic Ferromagnetism in ZnO:Co, Phys. Rev. Lett. **96**, 017203 (2006).

[45] A. Ney, T. Kammermeier, K. Ollefs, S. Ye, V. Ney, T. C. Kaspar, S. A. Chambers, F. Wilhelm, and A. Rogalev, Anisotropic paramagnetism of Co-doped ZnO epitaxial films, Phys. Rev. B **81**, 054420 (2010).

[46] G. B. Arfken, H. J. Weber, and F. E. Harris, *Mathematical Methods for Physicists: A Comprehensive Guide*, 7th ed. (Academic, Waltham, MA, 2013).

[47] G. O. Gomes, H. E. Stanley, and M. de Souza, Enhanced Grüneisen parameter in supercooled water, Sci. Rep. **9**, 12006 (2019).